PCCP

Accepted Manuscript

ROYAL SOCIETY OF CHEMISTRY

www.rsc.org/pccp

Journal Name

RSCPublishing

ARTICLE

Work Function Shifts of Zinc Oxide Surface upon Deposition of Self-Assembled Monolayers: A Theoretical Insight

Cite this: DOI: 10.1039/xoxxoooooox

Received ooth January 2012,
Accepted ooth January 2012

DOI: 10.1039/xoxxoooooox

www.rsc.org/

D. Cornil,[a] T. Van Regemorter,[a] D. Beljonne[a] and J. Cornil[a] ,

We have investigated at the theoretical Density Functional Theory level the way the work function of zinc oxide layers is affected upon deposition of self-assembled monolayers (SAMs). 4-terbutylpyridine (4TBP) and various benzoic acids (BA) were adsorbed on the apolar (10-10) ZnO and used as probe systems to assess the influence of several molecular parameters. For the benzoid acids, we have investigated the impact of changing the nature of the terminal group (H, CN, OCH3) and the binding mode of the carboxylic acid (monodentate versus bidentate) on the apolar (10-10) surface. For each system, we have quantified the contribution from the molecular core and the anchoring group as well as of the degree of surface reconstruction on the work function shift. For the benzoic acids, the structural reorganization of the surface induces a negative shift of the work function by about 0.3±0.15 eV depending on the nature of the binding mode, irrespective of the nature of the terminal function. The bond-dipole potential strongly contributes to the modification of the work function, with values in the range +1.2 to +2.0 eV. In the case of 4TBP, we further characterized the influence of the degree of coverage and of co-adsorbed species (H, OH, and water molecules) on the ZnO/SAM electronic properties as well as the influence of the ZnO surface polarity by considering several models of the polar (0001) ZnO surface. The introduction of water molecules in the (un)dissociated form at full coverage on the non-polar surface only reduces by 0.3-0.4 eV the work function compared to a reference system without co-adsorbed species. Regarding the polar surface, the work function is also significantly reduced upon deposition of a single 4BTP molecule (from -1.44 eV to -1.73 eV for our model structures), with a shift similar in direction and magnitude compared to the non-polar surfaces.

1. Introduction

The field of organic electronics relies on the use of organic conjugated molecules and polymers as active components in multilayered device applications such as light-emitting displays, solar cells or field-effect transistors.[1-3] Hybrid devices also proved to be of high interest to exploit the better charge transport properties of inorganic materials, as evidenced by the use of zinc oxide (ZnO) as interlayer or electrode in opto-electronic devices[4-14] or as nanoparticles in hybrid photovoltaic cells.[15-18] In all these devices, the key electronic processes (such as charge injection from metallic electrodes, charge recombination into light or light conversion into charges) occur at interfaces.[3] It has been largely documented at both the experimental and theoretical levels that the performance of organic-based opto-electronic devices can be enhanced by controlling the charge injection barriers between the organic semiconductors and metal / conducting metal oxides (such as ITO) via formation of interface dipoles triggered by the deposition of self-assembled monolayers (SAMs, *i.e.* an ordered two-dimensional layer of densely pack molecules) on their surface.[18-26] The interfacial properties of the ZnO surface can also be easily tuned by adsorption of a SAM layer[27, 28] ; for instance, the improvement in the efficiency of a polymer-based solar cell involving an ZnO/SAM electron transporting layer has been attributed to the reduction of the ZnO work function upon SAM treatment.[29] A lot of previous theoretical studies focused on metal/SAM interfaces to deeper investigate the molecular parameters controlling the work function shifts.[30-36] In contrast, much less attention has been given to the theoretical characterization of SAMs on metal oxide surfaces though DFT studies have been recently reported for SAMs based on phosphonic acid derivatives on polar ZnO and ITO surfaces[37-39] and on pyridine on ZnO.[40, 41]

In this context, the main goal of the present work is to investigate at the theoretical level the influence of self-assembled monolayers on the work function of both polar and apolar ZnO surfaces and to assess the impact of several molecular parameters. Our study encompasses SAMs made of benzoic acids terminated by three different substituents (H, CN

and OCH_3), see chemical structures in Figure 1(a-c) together with the dipole moment calculated in gas phase along the molecular axis. The z-component of the molecular dipole moment evolves from -2.15 D to +2.40 D among these three derivatives; the change in sign is expected to shift the work function in opposite directions, as demonstrated in a recent experimental work on benzoic acid derivatives on ZnO.[29] The influence of the binding mode of the carboxylic group on the work function shift will be also examined in details. Our study also involves the 4-terbutylpyridine (4TBP) molecule (Figure 1d) for a few fundamental reasons: (i) a pyridine anchoring group makes the analysis of the adsorption process easier since one atom has not to be eliminated during the deposition, as it is the case for the hydrogen atom of the carboxylic groups; (ii) the four systems under study allows to assess separately the influence of different terminal substituents and different anchoring groups on the work function shift; and (iii) this molecule is a standard additive in dye-sensitized solar cells.[42, 43]

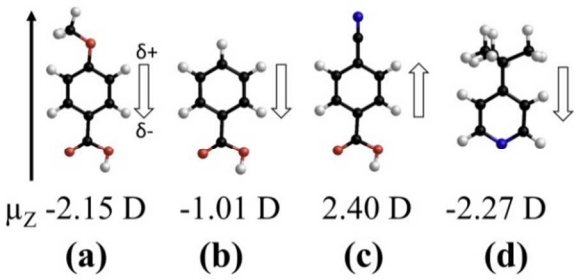

Fig. 1 Chemical structures of the benzoic acids with three different terminal groups (OCH_3 (a), H (b) and CN (c)) and of 4-tertbutylpyridine (d) considered as SAM-forming molecules in this study. We also report the value of the dipole moment along the molecular axis for the isolated molecules, as calculated at the DFT level with the PBE functional and a DZP basis set. The arrow represents the direction of the dipole moment along the z-axis (μz).

Regarding the ZnO surface, two main surface orientations are predominantly observed: the (10-10) non-polar and the (0001) or (0002) polar surface (see Figure 2).[44] While the non-polar surface is the most stable[45], the preferential growth direction of a wurtzite-like structure is generally taking place along the polar surface.[46, 47] Modeling the electronic properties of non-polar surface is rather straightforward and gives us a large flexibility to study the influence of several parameters such as the nature of the anchoring groups and terminal substituents, the influence of the degree of coverage or co-adsorbents such as water molecules, hydrogen atoms and hydroxyl groups, as will be done in the present study. In contrast, the modeling of the ZnO (0001) surface has long posed a significant challenge due to their electrostatic instability. Indeed, theoretically, bare Zn- and O-terminated polar surfaces show a disappearance of the band gap, a phenomenon referred to as metallization.[48] Various possible mechanisms stabilizing the polar ZnO surface have been suggested in previous studies.[49, 50] In a recent work, Li *et al*. have shown the important role played by -OH groups and vacancies on the actual electronic structure of the polar surface.[51] Based on this work, we have modeled the evolution of the electronic properties of the Zn-terminated or O-terminated polar (0001) surface including –OH and –H co-adsorbents and vacancies upon deposition of a SAM based on 4TBP in order to make a direct comparison with the non-polar (10-10) surface. In order to prevent the metallization problem, the bottom part of the ZnO slab is saturated by adding hydrogen atoms on the external oxygen atoms.[50, 51]

The paper has been structured as follows: Section 2 describes the theoretical methodology used in the present work while Section 3 collects all results. We will first discuss there the structural and electronic properties of the non-polar ZnO surface covered with BA and 4TBP, analyzing the impact of changing the anchoring group, the binding mode, and the terminal substituents as well as the influence of co-adsorbents. In the second part, we will exclusively focus on 4TBP molecule deposited on the different models of the polar Zn(0001) surface.

2. Methodology

All calculations were performed at the Density Functional Theory (DFT) level using the 3.0 version of SIESTA including periodic boundary conditions.[52, 53] The functional used was PBE initially developed by Perdew, Burke and Ernzerhof[54] with a double zeta basis set plus polarization orbitals (DZP). The surface model used for the (10-10) non-polar surface is made of 10 layers (thickness of 12.4 Å) with optimized a and b surface lattice vectors of 9.94 Å and 10.66 Å, respectively, which represent an elongation of only ~ 2% compared to the experimental bulk values.[55] For the (0001) polar surface, the Zn- and O-terminated models are similar to those recently investigated by Li *et al*.[51] in the absence of SAMs. These models are made of 12 layers (thickness of 13.8 Å) with a and b lattice vectors fixed during the geometry optimization to their experimental values of 6.50 Å and 5.63Å, respectively.[56] Note that in the case of the non-polar surface, only one side of the slab is modified by the adsorption of the SAM and the co-adsorbed species while the different models used for the polar surface involved adsorption of OH groups or H atoms at the bottom of the slab to avoid metallization effects. An additional double layer is there introduced to increase the separation between the two modified sides of the slab. The optimization of the structure and calculation of the electronic structure have been performed using a mesh cut-off of 190 Ry and a (3 × 3 × 1) k-point mesh. In order to fasten the optimization, the 6 uppermost layers are allowed to relax while the 4 (or 6) lowest layers are frozen for the non-polar (polar) systems. The electrostatic potential and charge density profile across the system were computed using a macroscopic average technique introduced by Baldereshi et al.[57] and implemented in Macroave, an utility linked to SIESTA. The projected densities of states (PDOS) were computed using the mprop program also available in the SIESTA utilities.

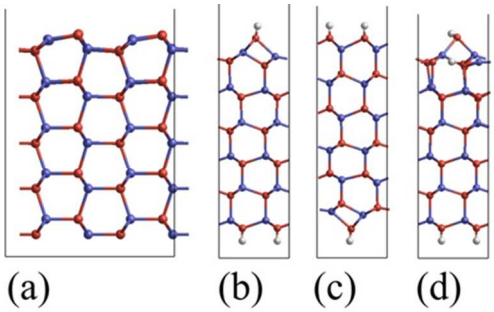

Fig. 2 Illustration of the ZnO surfaces used in this work. (a) Side view of the model used for the non-polar (10-10) ZnO surface. (b) shows the model used for the Zn-terminated polar surface fully covered by hydroxyl groups. (c) is the model used for the O-terminated polar surface half covered by hydrogen atoms. (d) is the Zn-terminated surface with one hydroxyl group and one Zn vacancy. The oxygen atoms are depicted in red, zinc atoms in blue and hydrogen atoms in white.

Since ZnO is experimentally known as intrinsically n-doped, the Fermi level is rather close to the conduction band minimum. Measurements performed by Jacobi *et al*. show that the work function (Φ) of an annealed surface is about 5.05 eV while the electronic affinity (χ) is around 4.60 eV. For the non-polar surface, they observed that χ and Φ become very close after a sufficiently long waiting time.[58] Since the position of the Fermi level just serves as a reference for zero energy and we are interested in the work function shift that is independent on the actual choice for the Fermi level energy, a reasonable choice is to associate the energy of the conduction band minimum (CBM) as a quasi-Fermi level. Therefore, we define the work function as the difference between the vacuum level (VL) and the CBM following Equation 1:

$$\Phi = VL - CBM \quad (1)$$

where VL is the value at which the electrostatic potential reaches a plateau in the vicinity of the surface and CBM is extracted from the computed density of states. Although the present procedure allows us to take into account implicitly the extrinsic n-type doping inherent to ZnO surfaces, it is clearly beyond the scope of the present paper to address the way dopants affect the vacuum level shift at the interface in presence of SAMs. As a matter of fact, a detailed study would require considering many different parameters such as the nature of the dopants, the doping density and the spatial distribution of the dopants at the interface. While recent works have demonstrated that the bond dipole can be affected by doping[59, 60], whether the vacuum level shift induced by SAM deposition is also sensitive to the presence of dopants remains a rather unexplored issue to be addressed in a forthcoming work. In the present work, Φ is calculated to be 4.47 eV for the relaxed bare ZnO (10-10) surface, which is consistent with experimental values of 4.5 eV.[58] Since the conduction band minimum is not affected by the adsorption of the molecules[61], the modification in the work function (ΔΦ) originates from a vacuum level shift generated by the presence of a dipole moment at the interface induced by the SAM.[34, 62] This interface dipole is generally decomposed in two main contributions: (i) the intrinsic dipole of the adsorbed molecule; and (ii) the dipole created by the formation of a chemical bond between the molecule and the surface. The variation of the electrostatic potential is directly related to the sum of these dipole moments according to the classical Helmholtz equation.[63-66] We will thus describe hereafter the variation of the work function ΔΦ as a combination of the potential modification induced by the intrinsic dipole moment of the molecule (ΔV_{SAM}) and the potential shift linked to the charge density rearrangement at the surface when the SAM is deposited. This latter quantity is generally refers to as the bond-dipole potential (BD).[33, 66, 67] The estimation of BD can be done numerically by resolving the Poisson equation on the basis of the charge density difference at the interface Δρ, as further described in the results.

Finally, we also need to take into account in the analysis that: i) the adsorption of the SAM can induce a geometrical restructuration of the surface, in contrast to the trends typically observed for metals; and ii) the ZnO surface already contains some co-adsorbents prior to the SAM deposition in the experimental conditions typically used.[44] This already modifies the work function of the ZnO surface by a quantity ΔV_{ZnO} compared to the reference bare surface.[68] We define this latter quantity as $\Phi^* - \Phi_{bare}$, with Φ* the work function of the ZnO surface calculated in the relaxed interface geometry after removing the SAM (BA or 4TBP) and Φ_{bare} the work function of the free relaxed ZnO surface, used as reference (calculated to be 4.47 eV) Altogether, the modification of the work function can thus be described by the addition of all these quantities:

$$\Delta\Phi = \Delta V_{SAM} + \Delta V_{ZnO} + BD \quad (2)$$

The relative contributions of all these components to the work function modification have been calculated and discussed in the following sections for the 4TBP (with and without co-adsorbed species) and for the BA derivatives. Note that in the case of the polar surface, the reference system is made of the ZnO surface plus the vacancies and/or co-adsorbed species introduced to avoid the metallization problems.

3. Results and discussion

3.1. (10-10) ZnO surface.

Figure 2a illustrates that the bulk structure below the (10-10) ZnO surface is constituted of Zn-O dimer rows. The geometry optimization points to a reconstruction of the top layer at the surface, with the cation moving below the anion. Naming Zn1, O1 and Zn2, O2 the atoms from the first and second layer respectively, the atomic displacement along the z-axis upon relaxation compared to the position in the bulk is calculated to be -0.23 Å for Zn1 ; +0.09 Å for O1 ; +0.13 Å for Zn2 and +0.01 for O2. This results into a tilt of the surface Zn-O dimers by about 7.8°, in good quantitative agreement with the results of other DFT approaches.[69-73] This reconstruction of the surface is induced by the reduction in the degree of coordination of the surface atoms compared to those in the bulk, which creates an occupied [empty] dangling bond on the anion [cation]. The magnitude of this relaxation is generally attributed to a competition between two limiting cases: dehybridization, *i.e.*, a change in the orbital shape (in a dominantly covalent bonded structure), versus charge-transfer effects from the cation towards the anion (in ionic solids).[72] In the case of ZnO, the moderate dimer rotation reflects the strong ionicity of the metal oxide.[74]

This surface reconstruction generates an intrinsic dipole of 1.97 Debye which is compensated in our periodic calculations by the presence of a dipolar correction along the z-axis to avoid self-interactions (*i.e.*, interactions of one slab with its images). This reconstructed surface has been referred to in the remaining as the bare ZnO surface and used in the calculations as a starting point for the deposition of 4TBP or BA derivatives.

3.2. BA and its derivatives on (10-10) ZnO.

Carboxylic acids form covalent stable bonds with metal oxide; the nature of this bond is known to be of ester- (monodentate adsorption) or carboxylate-type (bidentate adsorption)[75] so that theoretical studies made on carboxylic acid/ZnO interfaces generally involve different contact geometries.[76, 77] In this work, we modeled the adsorption of the carboxylic acid on the ZnO surface by considering and optimizing three main bonding modes (see Figure 3): (i) a monodentate mode (named BM1) where the anchoring between the carboxylic group and the metal oxide is made through the formation of an ester-type bond. In that case, a hydrogen bond is formed between one of the oxygen atom of the carboxylic group and the departing H atom which is attached on a peripheral surface oxygen atom;

Table 1 Adsorption energies, tilt angle (θ) and twist angle (φ) of BA with different terminal groups for the 3 binding modes considered.

	Monodentate		Bidentate				Chelate
	BM1.1	BM1.2	BM2.1	BM2.2	BM2.3	BM2.4	BM3
E_{ads} (kJ/mol)							
BA – OCH_3	-241.1	-208.9	-339.1	-313.4	-338.0	-301.9	-246.4
BA – H	-238.5	-221.8	-334.4	-331.4	-339.2	-309.0	-253.3
BA – CN	-237.9	-237.8	-321.7	-331.1	-337.3	-304.3	-244.0
θ (°)							
BA – OCH_3	27.8	12.5	27.7	22.9	3.1	4.7	14.1
BA – H	32.9	15.1	22.7	22.2	13.9	13.5	21.3
BA – CN	32.2	7.8	23.9	19.5	5.1	8.3	22.0
φ (°)							
BA – OCH_3	30.4	3.2	76.2	75.0	67.3	69.7	0.3
BA – H	35.5	2.6	68.4	86.0	54.6	65.5	8.0
BA – CN	32.0	1.5	52.7	86.1	70.8	73.5	0.1

(ii) a bidentate mode (BM2) with the two oxygen atoms of the carboxylic function bonded to two different surface Zn atoms; (iii) a bidentate chelating mode (BM3) with the two oxygen atoms of the carboxylic acid interacting with only one surface Zn atom. In all cases, the departing H atom is attached to a peripheral oxygen atom of the surface though different configurations can be distinguished based on the exact position of the hydrogen atom (thus rationalizing the terminology BM1.x and BM2.x used hereafter). This scheme for the fate of the departing hydrogen has also been used in previous theoretical investigations involving carboxylic acid/ZnO interfaces.[76, 77] A full relaxation of these structures leads finally to the seven configurations shown in Figure 3.

In the case of the monodentate binding mode, two configurations can be distinguished: BM1.1, where the departing hydrogen atom is attached to the surface O atom directly bonded to the surface Zn atom involved in the "ester-type" bond; and BM1.2, where the departing hydrogen is attached to an oxygen atom of the surface not bonded to the Zn atom of the ester bond. The configurations BM1.1 and BM1.2 illustrated in Figure 3 are the only two for which the monodentate mode is found to be conserved during the geometry relaxation. Other configurations have been tested with the hydrogen atom attached on each of the other oxygen atoms available on the surface; in each case, the geometry relaxation converges to one of the bidentate mode described below. For the bidentate mode, we have considered four configurations which differ by the position of the departing hydrogen, as shown in Figure 3. In this mode, two configurations (BM2.2 and BM2.3) display a hydrogen bond between the departed hydrogen and the two oxygen atoms of the carboxylic group while such a bond is not observed in BM2.1 and BM2.4 due to the increase in the distance between the respective atoms. Finally, for the chelate mode BM3, only one configuration was considered. Indeed, this mode appears to be more unstable compared to the monodentate or bidentate modes so that the geometry relaxations started from a chelate configuration have a large tendency to converge towards the two other modes. The BM3 structure shown in Figure 3 and included in this study was found as a local minimum in the relaxation towards the monodentate mode.

This structural analysis has been performed for the three BA derivatives varying by the nature of the terminal group (-H, -OCH3, and -CN, see Figure 1(a-c)). It is worth pointing out that the nature of the terminal group does not affect the binding geometry. The adsorption energies were calculated from the difference between the energy of the entire system and the sum of the energies of the free isolated molecule and free bare ZnO surface using expression (3):

$$E_{ads} = E_{ZnO\text{-}H/BA} - [E_{ZnO} + E_{BA\text{-}H}] \qquad (3)$$

where $E_{ZnO\text{-}H/BA}$ is the energy of the interface after geometry relaxation, E_{ZnO} the energy of the relaxed ZnO surface after removal of the adsorbate species and $E_{BA\text{-}H}$ the energy of the free molecule in the adsorption geometry with the departing hydrogen atom reattached to the terminal oxygen atom of the carboxylic function. Table 1 summarizes the adsorption energy for the different BA molecules in the several anchoring positions considered. A similar evolution of the adsorption energy with the binding mode is observed for the three BA molecules. The most stable contact geometries are found for the bidentate mode (BM2.x) while the chelate and monodentate modes are lying higher in energy by about 90 kJ/mol.

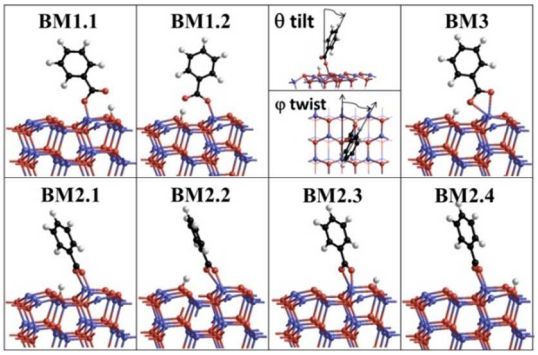

Fig. 3 Representation of the several binding modes of the benzoic acid on the non-polar ZnO surface. BM1.x corresponds to a monodentate mode, BM2.x to a bidentate mode, and BM3 to the chelate configuration. We also include a schematic representation of the θ tilt and φ twist angle defined in the text. Due to the symmetry of the unit cell exhibiting six identical Zn-O dimers, the Zn atom involved in the bonding has been selected randomly.

The highest stability of the bonding configurations involving the two carbon atoms of the carboxylic group is consistent with Fourier transform infrared attenuated total reflectance (FTIR-ATR) data obtained for ZnO nanotips functionalized with carboxylic acids which point to the disappearance of the C=O signature in the spectra.[75] The most stable geometry obtained for the BA molecules on the ZnO surface is characterized by bond lengths for the two C-O bonds in the range of 1.26-1.31 Å. For comparison, calculations performed on the isolated BA yield lengths of 1.23 Å and 1.37 Å for the C=O and C–OH bonds, respectively. This is consistent with the appearance of an electronic delocalization in the carboxylate function upon chemical anchoring. The length of the anchoring bonds (Zn-O) has also been analyzed for each binding mode. For a monodentate anchoring, small difference appears between the two geometries considered, with a Zn-O bond on the order of 1.98-2.00 Å for BM1.1 and 2.00-2.03 Å for BM1.2. A small elongation of the bond is observed with the bidentate BM2.1 → BM2.4 modes, with a bond length ranging from 2.01-2.12 Å. For the chelate mode (BM3), the anchoring bond length reaches values as high as 2.20-2.35 Å. The orientation of the electroactive substituent attached to the benzene ring of the BA can impact the surface electronic properties by modulating the direction of the dipole moment.[78] In this respect, we have estimated the tilt angle θ defined as the angle between the perpendicular to the surface and the axis connecting the carbon of the carboxylic group and the carbon supporting the substituent, see Table 1. The amplitude of the tilt angle depends on the nature of the binding mode while the nature of the substituents has a less pronounced impact. For the monodentate mode, a systematic reduction of the tilt angle prevails when going from BM1.1 to BM1.2. The θ angle lying around 30° in BM1.1 is reduced down to 8-15° in BM1.2. For the four models of the BM2 bidentate mode, tilt angles of ~20-28° are calculated for BM2.1 and BM2.2 and get reduced down to less than 15° for BM2.3 and BM2.4. For these latter modes, the nature of the substituents modulates in a more pronounced way the tilt angle, varying from 3-8° for BA-OCH_3 and BA-CN to 14° with BA-H. The different tilt angle between the two sets of structures (BM2.1/BM2.2 versus BM2.3/BM2.4) is likely to originate from the different localization of the departing hydrogen atom. As shown in Figure 3, the hydrogen atom is localized in BM2.1/BM2.2 on an oxygen atom not bonded to the Zn atom involved in the bonding while the opposite situation prevails for BM2.3 and BM2.4. The BM2.1/BM2.2 geometries allow for the formation of a hydrogen bond when the molecule is tilted while such a bond cannot be created for BM2.3/BM2.4 due to the unfavorable geometric conformation. Finally, the chelate mode BM3 displays tilt angles of ~15-20°, which are close to those observed in BM2.1/BM2.2. In addition to the θ angle, we also considered the rotation of the phenyl ring with respect to the ZnO surface. In order to quantify this parameter, we defined a twist angle φ as the angle between the projection of the plane passing through the phenyl ring and an axis passing through a vertical Zn-O dimer (see Figure 3). Using this definition, a twist angle of 0° is obtained when the phenyl ring is parallel to the Zn-O dimer. The results are collected in Table 1 and show a dependence of the twist angle on the binding mode. For the monodentate adsorption, starting from a geometry where the phenyl ring lies parallel to the Zn-O axis (φ = 0°), the optimization yields a final twist angle around 30-35° for each BA in the BM1.1 mode while the twist angle is negligible (φ between 1° and 3°) for the BM1.2 mode. This difference between the two monodentate binding modes originates from the position of the H adsorbed on the surface. Indeed, in the BM1.2. mode, all atoms participating to the anchoring, *i.e.*, the Zn atom from the surface, the carboxylate group and the adsorbed H making an hydrogen bond are localized in a same plane. However, for BM1.1, where the adsorbed H is localized closer to the Zn connected to the molecule, a torsion of the Zn-O-C-O angle occurs to generate an hydrogen bond; this induces a rotation of the phenyl ring by the same angle. The four modes considered for the bidentate adsorption yield large twist angles, in a range going from 50° to nearly 90°. The chelate mode behaves in a way similar to the BM1.2 mode, showing a small twist angle of the phenyl ring (see Table 1).

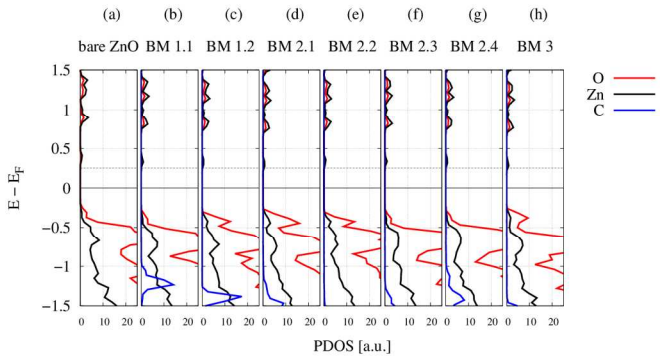

Fig. 4 Projected Density of States (PDOS) for the bare non-polar ZnO surface (a); with BA-H adsorbed on ZnO in a monodentate mode (b-c); in a bidentate mode (d-g) ; and in a chelate mode (h). The zero energy level corresponds to the Fermi level and the CBM is represented by a dash line.

After these structural considerations, we now turn to the shift of the work function Φ of the ZnO surface upon adsorption of the BA molecule for the various terminal groups and binding modes (see Supplementary information). The shift will be calculated with respect to the work function calculated for the bare (10-10) ZnO surface (4.47 eV) taken as a reference. We first computed the PDOS for each binding mode to investigate the influence of the binding mode on the CBM. As shown in Figure 4 for the BA-H molecule, the energy of the CBM is unaffected by the presence of the molecule and by a modification of the binding mode. Similar results are obtained for the three BA derivatives, thus indicating that a change in the terminal function does not affect the CBM position. The modification of the work function (ΔΦ) has been decomposed into the three components described previously: the potential shift arising from the free BA molecule (ΔV_{BA}), the surface restructuration (ΔV_{ZnO}) and the bond-dipole potential (BD). Since all structures exhibit a single hydrogen atom adsorbed on the surface, the BD was calculated by relying on a free standing hydrogen layer for the charge conservation:

$$\Delta\rho = \rho_{ZnO\text{-}H/BA} - [\rho_{ZnO} + \rho_{SAM} + \rho_{H}] \quad (4)$$

where $\rho_{ZnO\text{-}H/BA}$ is the charge density of the full system, ρ_{ZnO} the charge density of the free ZnO surface in its interface geometry, ρ_{SAM} the charge density of the free standing radical SAM in its interface geometry and ρ_H the charge density of the free standing hydrogen layer. Figure 5 points to significant differences in the work function shift depending on the nature of the terminal group and binding mode considered. The ZnO work function strongly increases with BA-CN, with shifts larger than 1.0 eV. For BA-OCH_3, the methoxy group induces an opposite behavior with a decrease of the work function down to -0.6 eV. In the case of BA-H, a small decrease in the work function is

observed with a maximum of -0.3 eV, though one binding mode induces an opposite behavior with an increase in $\Delta\Phi$ by about 0.2 eV. For each substituent, the variation of the work function fluctuates in a window between 0.4-0.6 eV depending on the nature of the binding mode.

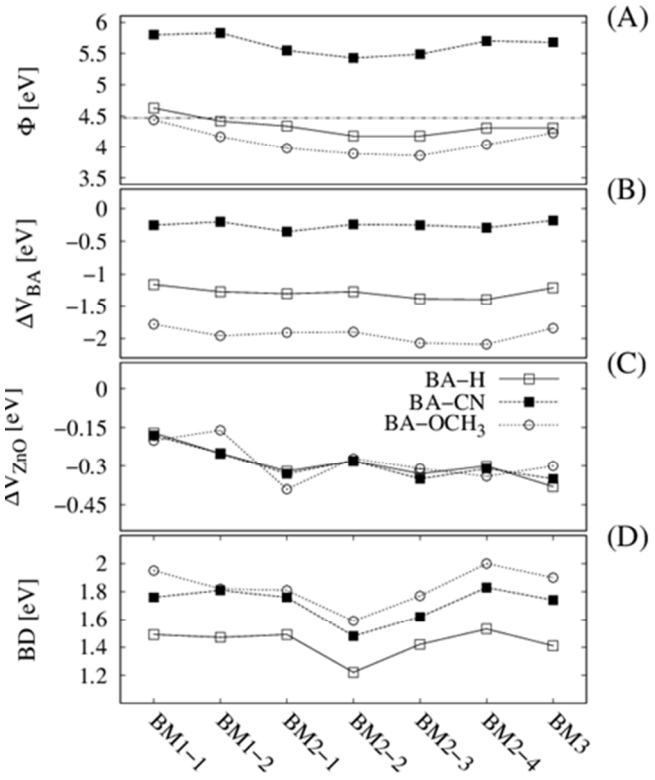

Fig. 5 Evolution of the different contributions to the work function shift for the BA molecules as a function of the binding mode. (A) Work function of the ZnO with the BA derivatives adsorbed on it; the horizontal dashed line represents the work function of the bare ZnO (4.47 eV). (B) Potential shift due to the free SAM in its interface geometry. (C) Contribution of surface restructuration upon SAM adsorption. (D) Amplitude of the BD potential.

The potential shift associated to the structural reorganization of the ZnO surface (ΔV_{ZnO}) is found to be slightly negative in all cases. Similar results are found for each BA compound in a given binding mode, see Figure 5 (C) indicating that the surface restructuration is largely unaffected by a change in the chemical function on top of the phenyl ring. This contribution slightly decreases (from *ca*. -0.2 eV to ca. -0.3 eV) going from the monodentate binding mode to the others.

The potential shift arising from the molecular part, ΔV_{BA}, is directly connected to the dipole moment of the molecule (in its radical form) perpendicular to the surface following the Helmholtz equation. The chemical functionalization of the benzoic acid thus provides an easy way to tune this quantity and hence the total work function shift. The benzoic acid used as reference (BA-H) is characterized by a ΔV_{BA} value ranging from -1.16 eV to -1.39 eV depending on the binding mode. Since we calculate ΔV_{BA} using the free standing radical SAM in its interface geometry, the differences among the various binding modes reflects small variations in the tilt and twist angle of the molecule, as discussed before. By substituting the top hydrogen atom by the electron-donating methoxy group, we further increase the ΔV_{BA} up to values between -1.78 eV and -2.09 eV depending on the binding mode. The opposite behavior prevails upon introduction of the electron-withdrawing cyano group which reduces ΔV_{BA} in a range between -0.18 and -0.35 eV, *i.e.* a drop of about 1 eV compared to the BA-H results. However, it is interesting to point out that, despite this large shift, the substitution of the hydrogen atom by a CN group does not reverse the direction of the total molecular dipole moment since the potential shift remains negative in the free standing SAM (actually, the CN substituent does change the sign of the dipole moment for the isolated neutral molecule and not for the isolated radicals). Moreover, for BA-CN, the contribution of the molecular backbone to the total work function modification (on the order of -0.3 eV) is similar to that associated to the surface reconstruction. Altogether, this indicates that the large value of $\Delta\Phi$ computed for BA-CN mainly originates from the last component, *i.e.*, the BD potential.

Figure 5 (D) shows the variation of the BD potential as a function of the binding mode for the three SAM species. This parameter scales in between 1.2 eV and 2.0 eV for the investigated structures. The profiles of the charge density difference have been calculated for each structure and are shown in Figure 6. Integration of these profiles highlight that ~ 0.3 |e| are transferred from the molecule to the ZnO surface. The amount of charge transferred appears to be very similar whatever the nature of the binding mode and results from an interplay between: i) a gain of electron for the oxygen atoms of the carboxylic group, through Zn-O bonds; and b) a loss of electron resulting from the transfer of the hydrogen to the ZnO surface to generate a hydroxylic group (see Supplementary information). Note that the bond dipole reflects the charge reorganization at the interface upon adsorption but does not necessarily correlate with the net amount of charge transferred between the molecule and the metallic electrode.[67] It is therefore possible to observe similar charge transfer processes at the interface though with different amplitudes of the bond dipole.

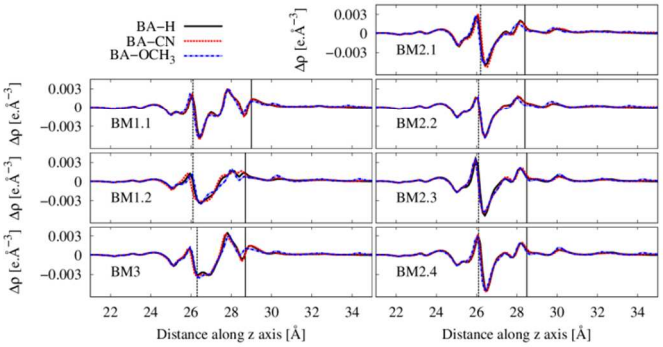

Fig. 6 Profile of the charge density difference for BA-H, BA-CN and BA-OCH3 for each binding mode. The dashed line represents the position of the top ZnO layer and the plain line the position of the carbon atom of the carboxylate group.

To conclude this first section, we have shown for BA derivatives on the non-polar surface that the modification in work function reflects the nature of the terminal group. Indeed, a $\Delta\Phi$ of around +1.0 eV is obtained when introducing strong electron acceptor like CN moeities, while $\Delta\Phi$ scales in between +0.2eV and -0.5 eV for the other two derivatives (BA-OCH3 and BA-H). This work function change has been decomposed into the following three main components: i) the intrinsic dipole moment of the molecule (ΔV_{BA}) ii) the anchoring bond (BD) and iii) the structural reorganization of the interface (ΔV_{ZnO}). For this latter quantity, we found a negative shift around 0.3±0.15 eV depending on the nature of the binding mode but independently of the nature of the terminal group. The

molecular contribution (ΔV_{BA}) is associated with the dipole moment of the molecule through the Helmholtz equation. Thus, the evolution of this quantity reflects the reorientation of the molecular dipole *i.e.* a change in the SAM geometry. It appears from our calculation that this quantity is only slightly affected by the nature of the binding mode with variations within a narrow range of 0.2 eV. Finally, the bond-dipole potential is observed to strongly contribute to the work function shift, with values going from +1.2 eV to +2.0 eV.

3.3. 4TBP on (10-10) ZnO.

Figure 7 summarizes the different surfaces and co-adsorbed species investigated for the 4TBP monolayer on ZnO. In a first step, a single 4TBP molecule was adsorbed without other species on the bare ZnO surface through the formation of a Zn-N bond. A second molecule was then added in the unit cell to explore the influence of molecular density (*i.e.*, degree of coverage) on the calculated electronic properties. Finally, different co-adsorption species (hydrogen, hydroxyl groups and water molecules) were adsorbed in addition to a single 4TBP.
A geometry optimization was carried out for each system by relaxing the adsorbed species (4TBP and co-adsorbed species if present on the surface) and the top 6 layers of ZnO. In each case, the adsorption energy was computed following the expression:

$$E_{ads} = E_{ZnO/4TBP} - [E_{ZnO} + E_{4TBP}] \qquad (5)$$

where $E_{ZnO/4TBP}$ is the energy of the full system after relaxation, E_{ZnO} the energy of the zinc oxide surface in its interfacial geometry without the SAM (but containing the co-adsorbents if present) and E_{4TBP} the energy of the free 4TBP in its interfacial geometry. The adsorption energies computed for each structure are compiled in Table 2 and are discussed in the following sections.

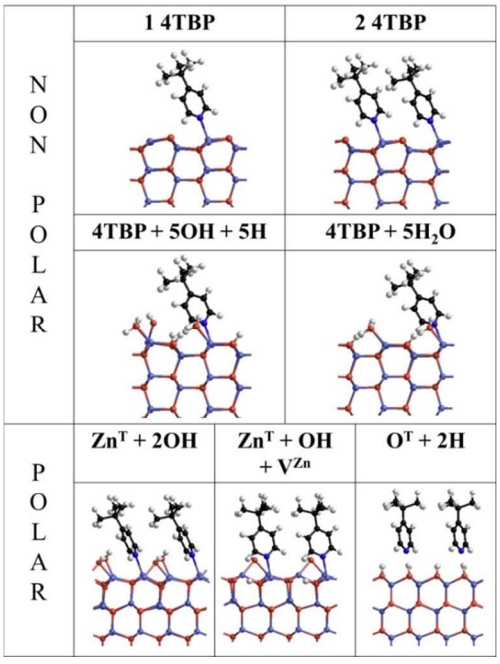

Fig. 7 Side view representation of the structures investigated for 4TBP on non-polar and polar surfaces of ZnO. The notation above each picture is used throughout the text and in Table 2 to refer to the corresponding system.

3.3.1. Single 4TBP. When a single 4TBP molecule is adsorbed without other species on the ZnO surface through the formation of a Zn-N bond. The adsorption energy is computed to be -146.7 kJ/mol which is close to the binding energy of 112 kJ/mol measured experimentally by Wöll *et coll.*[41] The equilibrium geometry displays an N-Zn distance of 2.14 Å, close to the 2.06 Å observed for a N-Zn bond in a pyridine-zinc complex via x-ray diffraction experiments.[79] In order to characterize the geometry of the SAM, we have defined the tilt angle as the angle between an axis perpendicular to the ZnO surface and an axis connecting the nitrogen atom and the top carbon atom of the aromatic cycle. Using this definition, the tilt angle of 4TBP is calculated to be 22.2°, which is consistent with a proposed model deduced from near-edge x-ray adsorption fine structure (NEXAFS) data for the pyridine molecules on ZnO (10-10) with a tilt angle of 19°.[80]
In the presence of a single 4TBP molecule per unit cell, Φ is calculated to drastically drop by -1.40 eV (Φ = 3.07 eV). The ΔV_{SAM} contribution induced by the intrinsic dipole moment of 4TBP is calculated to be -0.70 eV and the BD potential has an equal contribution with a value of -0.71 eV. In the case of pyridine/ZnO interface, BD is calculated from the charge density difference as:

$$\Delta\rho = \rho_{ZnO/4TBP} - [\rho_{ZnO} + \rho_{SAM}] \qquad (6)$$

where $\rho_{ZnO/4TBP}$, ρ_{ZnO} and ρ_{SAM} correspond to the charge densities of the relaxed interface, the ZnO surface and the 4TBP free SAM layer in their interfacial geometry (the co-adsorbed species remain on the ZnO surface when they are present).
In view of the calculated total work function modification of -1.40 eV compared to the BD and ΔV_{SAM} components, the contribution of the surface restructuration appears to be negligible here (+0.01 eV).

3.3.2. Influence of molecular density. The increase in the surface molecular density was achieved by the addition of a second 4TBP molecule on the ZnO surface. From the size of the optimized unit cell (a = 9.94 Å and b = 10.66 Å), we can estimate the surface density to be of 1 molecule per 53.0 Å². In this case, the adsorption energy per molecule gets slightly lower (-130.6 kJ/mol versus -146.7 kJ/mol for the single molecule). The Zn-N bond lengths are calculated to be 2.13 Å and 2.14 Å and the tilt angles 22.2° and 25.0°. This indicates that the addition of a second 4TBP molecule in the unit cell has only a minor impact on the geometric parameters of the SAM.
For our unit cell, the work function shift amounts to -2.15 eV. Recent experimental results and DFT calculations for the pyridine/ZnO(10-10) interface report a work function shift around -2.9 eV.[40] The large variation between these two values

Table 2 Adsorption energy of 4TBP on the various non-polar and polar ZnO surfaces under study (see Figure 7 for the notation).

Surface orientation and termination		E_{ads} (kJ/mol)
(10-10)	1 4TBP	-146.7
	2 4TBP	-130.6
	1 4TBP + 5OH + 5H	-153.0
	1 4TBP + $5H_2O$	-171.4
(0001)	Zn^T + 2 OH	-64.1
	O^T + 2 H	-107.9
	Zn^T + OH + V^{Zn}	-112.1

can be explained by the difference in the degree of molecular coverage (a ratio of one pyridine molecule per 3 surface Zn atoms in our study compared to a ratio at full coverage of one pyridine molecule per 2 surface Zn atoms in Ref. 40). The evolution of the experimental work function shift with the coverage ratio reported in Ref 40 would yield a $\Delta\Phi$ value close to -2.5 eV at the coverage density used in our calculations, thus providing a better consistency between the two sets of data.
The variation of work function corresponds to a decrease of -1.07 eV per molecule while a decrease of -1.40 eV was previously calculated in the case of a single 4TBP in the unit cell. This difference originates from the depolarization effects linked to dipole-dipole interaction effects that tend to reduce the value of the individual dipoles when the molecular density is increased.[81-84] The difference of 0.33 eV between the (1 4TBP) and (2 4TBP) systems is associated to a drop by ~23% of the amplitude of the interface dipole moment associated to a single 4TBP molecule, in agreement with typical values observed for alkanethiolated and conjugated SAMs.[36, 81, 85] We now turn to the decomposition of $\Delta\Phi$ into its different components. The ΔV_{4TBP} and BD potential shifts for the (2 4TBP) system are calculated to be -1.15 eV and -0.98 eV, respectively. Since there are two molecules per unit cell, this represents a value per molecule of -0.58 eV for ΔV_{4TBP} and -0.49 eV for BD, to be compared to ΔV_{4TBP} = -0.70 eV and BD = -0.71 eV for the (1 4TBP) system; this represents a degree of depolarization of ~17% for ΔV_{4TBP} and ~31% for BD.

3.3.3. Influence of co-adsorbents. It is well known experimentally that water rapidly covers ZnO surfaces, even in ultra-high vacuum where water is the main constituent of residual gases.[44] In addition, it was previously shown by different spectroscopic techniques and theoretical calculations that water molecules partially dissociate on the surface.[45, 86, 87] The presence of adsorbed species on the ZnO surface can strongly affect its electronic structure; in particular, a metallization of the (10-10) ZnO was reported both experimentally and theoretically when adsorbing species like hydrogen atoms, methanol or water molecules.[88, 89] Dealing with co-adsorption on the 4TBP/ZnO interface thus requires much care since any possible shift in the position of the CBM should be accounted for to estimate the total work function shift. In order to understand how these co-adsorbed species affect the global change in the work function induced by the adsorbed monolayers, we have considered here two different models where we have fully covered the ZnO surface unit cell containing one 4TBP molecule by water molecules in their dissociated (4TBP + 5OH + 5H) and intact (4TBP + 5H2O) forms. Figure 8 reports the density of states of the different systems and illustrates that the position of CBM for the bare ZnO surface is not affected by the adsorption of 4TBP and by the co-adsorption of 5 (un)dissociated water molecules. Note that a partial coverage of the surface by OH or H leads to a deep modification in the density of states of the ZnO surface (*i.e.*, the appearance of a metallic character is observed) and will not be explored in the present study.

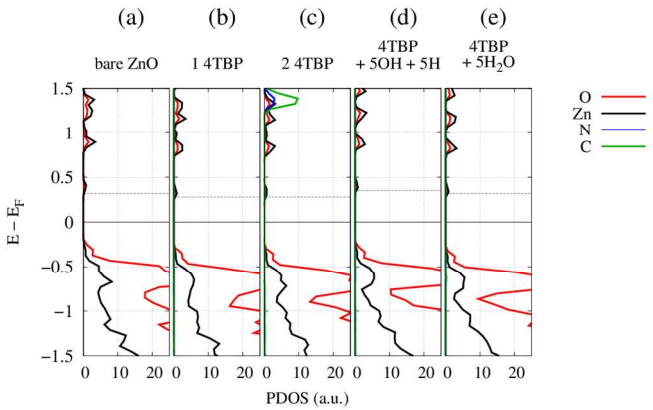

Fig. 8 Projected Density of States (PDOS) for: (a) the bare non-polar ZnO surface; (b-c) a ZnO surface containing 1 (or 2) 4TBP per unit cell and; (d-e) 1 4TBP with 5 dissociated or intact molecules. The zero energy level corresponds to the Fermi level while the CBM is represented by the dashed line.

The adsorption energy is reported in Table 2 for the two models. Compared to the 4TBP/ZnO interface with no co-adsorbents (E_{ads} = -146.7 kJ/mol), the interfaces carrying co-adsorbed species show an increase in the adsorption energy, with values of -153.0 kJ/mol calculated for the (4TBP + 5OH + 5H) model and -171.4 kJ/mol for (4TBP + $5H_2O$). The presence of the co-adsorbents has only a small impact on the geometric parameters of 4TBP deposited on the ZnO surface. Indeed, the length of the Zn-N bond is still in a range between 2.10-2.13 Å and the tilt angle is calculated to be 25.5° (4TBP + 5OH + 5H) and 27.8° for (4TBP + $5H_2O$), to be compared to 22.2° for the single 4TBP molecule. The work function shift calculated for the two models are reported in Table 3. In comparison to the work function of a ZnO surface covered by a single 4TBP molecule (3.07 eV), the systems including five un(dissociated) water molecules exhibit quite rather similar values, 3.31 eV and 3.45 eV, respectively. A full passivation of the surface by water molecules has thus no major impact on the calculated electronic properties. The BD contribution has similar value for the ZnO surface covered by 5 undissociated or 5 dissociated water molecules present (-0.61 eV versus 0-.77 eV) and has also the same order of magnitude as the value calculated in absence of co-adsorbents (-0.71 eV). This demonstrates that the nature of the bonding between ZnO and 4TBP is not affected by the presence of the water molecules and that the shift in the work function induced by the co-adsorbents (on the order of 0.3 eV) is mostly driven by changes in the surface restructuration, see Table 3.

In this second section, we have thus characterized the work function shift induced by the 4TBP (alone or with co-adsorbent species) on the non-polar surface of ZnO. For 4TBP alone on the surface, we calculated a strong modification of the work function $\Delta\Phi$ by -1.40 eV. A detailed investigation shows that both bond and molecular dipoles shift the vacuum level in the same direction and with a similar amplitude (-0.70 eV) while the structural reorganization is negligible. The

Table 3 Work function shift of the ZnO surface upon addition of 4TBP (with and without co-adsorbed species). The modification of the work function is decomposed in its different components. All values are in eV.

Surface	Φ	$\Delta\Phi$	ΔV_{4TBP}	BD	ΔV_{ZnO}
Bare ZnO	4.47	-	-	-	-
1 4TBP	3.07	-1.40	-0.70	-0.71	+0.01
2 4TBP	2.32	-2.15	-1.15	-0.98	-0.02
1 4TBP + 5OH + 5H	3.45	-1.02	-0.69	-0.77	+0.44
1 4TBP + $5H_2O$	3.31	-1.16	-0.66	-0.61	+0.11

increase of the areal molecular density by a factor two boosts the work function shift up to -2 eV while the amplitude of the molecular dipole moment is reduced by 20 to 30% owing to depolarization effects. We finally considered the impact of co-adsorbent species, namely water molecules in the (un)dissociated form, at full coverage on the surface. We calculate a reduction in the amplitude of the ZnO work function shift by 0.3-0.4 eV compared to the system without co-adsorbed species used as reference. This modification mainly stems from the additional dipole moment carried by the co-adsorbent, which contributes to the ΔV_{ZnO} in the opposite way compared to the ΔV_{4TBP} and BD components. These latter two quantities remain quasi unaffected by the introduction of co-adsorbent molecules in comparison to the reference system (change by less than 0.05 eV for ΔV_{4TBP} and ~0.1 eV for BD).

3.4. 4TBP on polar ZnO.

In this last Section, we will compare how the deposition of 4TBP molecules affects the work function of non-polar versus polar ZnO surfaces. This study will only focus of 4TBP since the absence of departing H atoms makes the analysis more straightforward. For the polar surface, we have considered both Zn- and O-terminated surfaces (the notations Zn^T and O^T used in this part make reference to these two polar surfaces) using the representative models developed in a recent theoretical work of Li *et al*[51] where metallicity problems are avoided; more specifically, and using the nomenclature in their paper, we focused on Model-1 and Model-4. Model-1 consists in a surface unit cell covered by two hydroxyl groups obtained by adding two hydroxyl groups on Zn atoms for Zn^T (Figure 2b) or two hydrogen atoms on oxygen atoms for O^T surface (Figure 2c); Model-4 is the most stable final geometry obtained when starting from Model-1 (zinc-terminated) and introducing one vacancy in oxygen and one vacancy in zinc in the top layer. During the optimization process, one hydroxyl group migrates to the position of the oxygen vacancy, leading to the structure illustrated in Figure 2d. The adsorption energy has been calculated in a way similar to that used for the non-polar surface on the basis of expression (5). The adsorption energies for the Zn^T (+ 2OH) and O^T (+ 2H) models are very different, with values of -107.9 kJ/mol for the O^T surface and only -64.1 kJ/mol for the Zn^T surface. This contrasts, however, with recent experimental data showing that pyridine gets adsorbed on Zn^T surface at room temperature while no adsorption is observed for O^T surfaces.[41] The theoretical results are fully explained by the fact that 4TBP is stabilized on O^T surfaces by a hydrogen-bond between the nitrogen of 4TBP and an adjacent hydrogen atom; the length of this O-H…N bond is measured to be 1.52 Å. However, in the case of the Zn^T surface, the presence of the two hydroxyl groups reduces the strength of the anchoring since the Zn-N distance is measured to be only 2.34 Å while a value of 2.14 Å is calculated for a single 4TBP molecule on the non-polar ZnO surface. Interestingly, an opposite trend prevails when introducing a Zn vacancy; we obtain indeed in this case adsorption energies of -91.4 kJ/mol for O^T and -112.1 kJ/mol Zn^T. This indicates that knowing the exact nature of the surface is a prerequisite to make reliable comparisons between theory and experiment. The calculated tilt angle is reduced by about 10 degrees moving from Zn^T to O^T surfaces, with 19.4° for (Zn^T + 2OH) and 7.8° for (O^T + 2H), to be compared to 22.2° for 4TBP on the non-polar surface. This reduction of the tilt angle is also observed when introducing a Zn vacancy in the (Zn + OH + V_{Zn}) model, with a value of 12.2°.

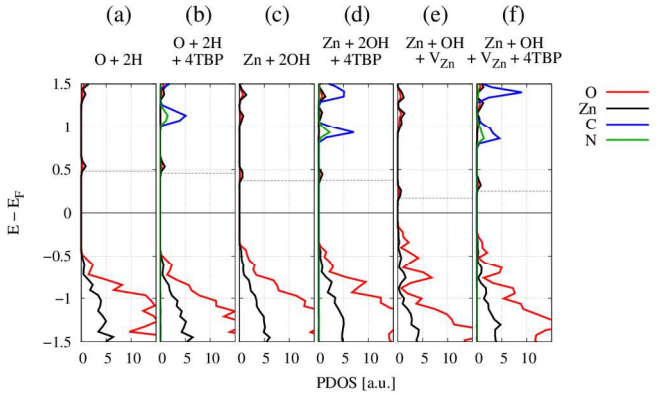

Fig. 9 Projected Density of States (DOS) for the ZnO polar models with and without 4TBP. The zero energy is set to the Fermi level and the position of the CBM is indicated by the dashed line.

Figure 9 represents the calculated PDOS for the several polar model surfaces considered in this work with and without the 4TBP on them. The adsorption of 4TBP has a slight impact on the position of the CBM. In contrast, the introduction of the Zn vacancy induces the appearance of a "tail-like" feature in the top of the valence band.[51] The work function has been computed for 4TBP adsorbed on the O^T and Zn^T models described earlier and decomposed into its molecular (ΔV_{4TBP}), bonding (BD) and surface reconstruction (ΔV_{ZnO}) components. As previously shown by Li *et al*., the presence of hydroxyl groups or vacancies at the surface can have a huge impact on the work function of ZnO, which changes by up to 1.5 eV depending on the chosen model. Though using a different DFT formalism, such a trend is also fully recovered here since the work function varies from 2.98 eV to 3.89 eV among the three model surfaces (see Table 4).

The introduction of a Zn vacancy in the Zn^T structure induces a significant shift of the work function by *ca*. 0.9 eV (from 2.98 eV for Zn^T + 2OH to 3.89 eV for Zn^T + OH + V_{Zn}). The vacancy model also improves significantly the quantitative agreement with the experimental value of the work function of a ZnT terminated surface, lying around 4 eV.[90] When adsorbing a single 4TBP molecule, a decrease in the work function is observed for all models; the surfaces without vacancy yield a work function shift of -1.73 eV (O^T + 2H) and -1.44 eV (Zn^T + 2OH) whereas a shift as high as -2.25 eV is calculated in the presence of the Zn vacancy.

In order to make a direct comparison with the value obtained for the non-polar surface, we first have to account for the

Table 4 Work functions for the model polar ZnO surfaces with and without 4TBP adsorbed on them. All values are in eV.

Model	Φ_{ZnO}	Φ_{SAM}	$\Delta\Phi$	ΔV_{4TBP}	BD	ΔV_{ZnO}
O^T + 2 H	3.35	1.62	-1.73	-1.50	-0.50	+0.27
Zn^T + 2 OH	2.98	1.54	-1.44	-1.51	-0.18	+0.25
Zn^T + OH + V_{Zn}	3.89	1.64	-2.25	-1.61	-1.20	+0.56

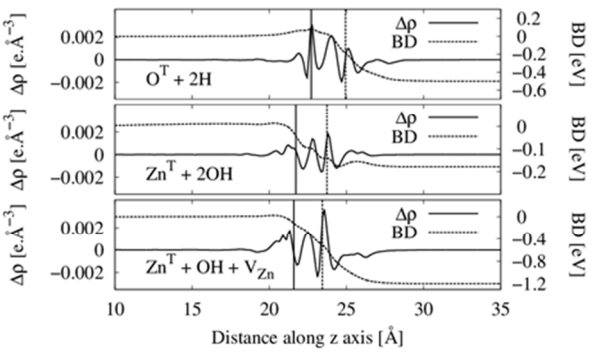

Fig. 10 Plane averaged charge density difference (Δρ) and corresponding bond-dipole potential (BD) for the three polar models used in this work. The position of the ZnO top layer and nitrogen of 4TBP are indicated by a straight line and a dashed line, respectively.

significant difference in molecular areal density between the non-polar and polar models involved in this work. Indeed, for the 4TBP/ZnO(10-10) interface, the surface per molecule is estimated to be ~106 Å^2 (1 4TBP) and ~53 Å^2 (2 4TBP), which represents a molecular areal density of N = 9.4 1013 and N = 1.9 10^{14} molecules/cm², respectively. In the polar models, the lattice vectors (a = 6.50Å; b = 5.63Å) leads to a density of N = 2.7 10^{14} molecule/cm². The contribution of ΔV_{4TBP} is found to be similar for the three polar models (with values around -1.5 to -1.6 eV) and much more negative than the corresponding amplitudes for the non-polar surface (-0.70 eV for a single 4TBP and -1.15 eV for two 4TBP). According to the classical Helmholtz formula, ΔV is proportional to N μ, with N the molecular areal density and μ the dipole moment of the individual molecules in the SAM. The evolution of ΔV_{4TBP} thus results from a subtle interplay between the increase of N and the associated change in the individual dipole moments due to the depolarization effects. The calculated BD potentials vary significantly as a function of the nature of the surface, with values of -0.50 eV for the O^T surface and -0.18 eV for the Zn^T surface, in both cases without the vacancy; the introduction of the Zn vacancy strongly impacts BD that reaches a value of -1.20 eV *i.e.* a difference of 1 eV compared to the systems without vacancy. This different behavior is visualized by the charge reorganization profiles which have been plotted in Figure 10. The introduction of the vacancy strongly modulates the charge profile in the part of the plot corresponding to the top of the ZnO surface and nitrogen atom of 4TBP. The integration of the charge profile between these two positions yields a difference by a factor 2 between the Zn^T model with and without vacancy, with the higher charge density found in the former case. The presence of the vacancy also influences the degree of reconstruction of the ZnO surface upon adsorption of 4TBP; without vacancy ΔV_{ZnO} is similar for the two polar ZnO models, +0.27 eV for O^T and + 0.25 eV for Zn^T while it amounts to +0.56 eV for the (Zn^T + OH + V_{Zn}) model.

Conclusions

In this work, we have investigated at the theoretical DFT level the way the work function of ZnO surfaces can be modulated by the deposition of self-assembled monolayers. We have focused on benzoic acid (BA) derivatives and 4-terbutylpyridine (4TBP) to assess the influence of many different parameters governing experimental measurements: (i) the nature of the anchoring group (pyridine for 4TBP versus carboxylic acid for the BA derivatives; (ii) the binding mode to the surface for the BA derivatives; (iii) the influence of electroactive substituents attached to the conjugated backbone of the SAM-forming molecules; (iv) the degree of coverage; (v) the presence of water molecules as co-adsorbents or vacancies on the surface; and (vi) the polarity of the surface. The shift in the work function has been systematically decomposed into its three components associated to: (i) the molecular dipole of the backbone; (ii) the bond dipole linked to the electronic reorganization triggered by the adsorption process; and iii) the structural reorganization of the top layer induced upon deposition of the SAM-forming molecules and by the introduction of co-adsorbents and vacancies.

For BA derivatives on the non-polar surface, the modification of the surface work function reflects the nature of the terminal function, with ΔΦ around +1.0 eV for BA-CN while ΔΦ scales in between +0.2eV and -0.5 eV for the two other derivatives (BA-OCH_3 and BA-H). The structural reorganization induces a negative shift around 0.3±0.15 eV depending on the nature of the binding mode but independently of the nature of the terminal function. The binding mode has a limited impact for the ΔVBA component and is on the order of 0.2 eV. The bond-dipole potential strongly contributes to the work function shift, with values in a range between +1.2 eV and +2.0 eV.

For 4TBP alone on the non-polar surface, the bond and molecular dipoles shift the vacuum level in the same direction and induce a strong modification of the work function ΔΦ by -1.40 eV; when using pyridine as the anchoring group, the structural reorganization is very small (nearly close to 0 eV). The work function shift can climb up to -2 eV when increasing the areal molecular density by a factor of two; the degree of depolarization effects (around 20-30%) has the same order of magnitude as that typically calculated for molecules deposited on metallic surfaces. The introduction of water molecules in the (un)dissociated form at full coverage on the surface only reduces by 0.3-0.4 eV the work function compared to a reference system without co-adsorbed species. In the last part, we have also computed the change in the work function of the polar ZnO (0001) surface using models including partial hydroxylation and vacancies in order to reflect actual measurement conditions and avoid metallicity problems. The work function is also significantly reduced in this case upon deposition of a single 4BTP molecule (in a range between -1.44 eV and -1.73 eV for our models), with a shift similar in direction and magnitude compared to the non-polar surfaces. All together, this manuscript has provided useful guidelines to help gaining a better understanding and control of the electronic properties of hybrid interfaces in opto-electronic devices.

Acknowledgements

The authors acknowledge Mats Fahlman and Parisa Sehati (University of Linköping) for sharing with us UPS data on ZnO/SAM interfaces and Hong Li (Georgia Institute of Technology) for stimulating discussions. This work has been supported by the European Project MINOTOR (FP7-NMP-228424), the Interuniversity Attraction Pole program of the Belgian Federal Science Policy Office (PAI 6/27), and the Belgian National Fund for Scientific Research (FRS-FNRS). J.C. and D.B. are FNRS Research Directors.

Notes and references

[a] Laboratory for Chemistry of Novel Materials, University of Mons (UMons), Place du Parc 20, Mons 7000, Belgium.

Electronic Supplementary Information (ESI) available: [Table with the decomposition of the work function shift for the BA compounds. Three-dimensional mapping of the charge density difference for BA/ZnO and 4TBP/ZnO interfaces.]. See DOI: 10.1039/b000000x/

1. H. Ma, H.-L. Yip, F. Huang and A. K. Y. Jen, *Adv. Funct. Mater.*, 2010, **20**, 1371-1388.
2. S. Allard, M. Forster, B. Souharce, H. Thiem and U. Scherf, *Angew. Chem. Int. Ed.*, 2008, **47**, 4070-4098.
3. N. Koch, *ChemPhysChem*, 2007, **8**, 1438-1455.
4. H. J. Bolink, E. Coronado, J. Orozco and M. Sessolo, *Adv. Mater.*, 2009, **21**, 79.
5. H. J. Bolink, E. Coronado and M. Sessolo, *Chem. Mater.*, 2009, **21**, 439.
6. H. J. Bolink, H. Brine, E. Coronado and M. Sessolo, *J. Mater. Chem.*, 2010, **20**, 4047.
7. H. J. Bolink, H. Brine, E. Coronado and M. Sessolo, *Adv. Mater.*, 2010, **22**, 2198.
8. B. A. Bailey, M. O. Reese, D. C. Olson, S. E. Shaheen and N. Kopidakis, *Org. Electron.*, 2011, **12**, 108.
9. M. T. Lloyd, R. P. Prasankumar, M. B. Sinclair, A. C. Mayer, D. C. Olson and J. W. P. Hsu, *J. Mater. Chem.*, 2009, **19**, 4609.
10. T. C. Monson, M. T. Lloyd, D. C. Olson, Y. J. Lee and J. W. P. Hsu, *Adv. Mater.*, 2008, **20**, 4755.
11. D. C. Olson, Y. J. Lee, M. S. White, N. Kopidakis, S. E. Shaheen, D. S. Ginley, J. A. Voigt and J. W. P. Hsu, *J. Phys. Chem. C*, 2007, **111**, 16640.
12. D. C. Olson, S. E. Shaheen, R. T. Collins and D. S. Ginley, *J. Phys. Chem. C*, 2007, **111**, 16670.
13. D. C. Olson, Y. J. Lee, M. S. White, N. Kopidakis, S. E. Shaheen, D. S. Ginley, J. A. Voigt and J. W. P. Hsu, *J. Phys. Chem. C*, 2008, **112**, 9544.
14. E. D. Spoerke, M. T. Lloyd, E. M. McCready, D. C. Olson, Y. J. Lee and J. W. P. Hsu, *Appl. Phys. Lett.*, 2009, **95**, 213506.
15. L. Wang, X. Zhang and K. Chen, *CrystEngComm*, 2013, **15**, 4860-4864.
16. M.-C. Kao, H.-Z. Chen, S.-L. Young, C.-C. Lin and C.-Y. Kung, *Nanoscale Research Letters*, 2012, **7**, 260.
17. K. K. Wong, A. Ng, X. Y. Chen, Y. H. Ng, Y. H. Leung, K. H. Ho, A. B. Djurišić, A. M. C. Ng, W. K. Chan, L. Yu and D. L. Phillips, *ACS Applied Materials & Interfaces*, 2012, **4**, 1254-1261.
18. H.-L. Yip, S. K. Hau, N. S. Baek, H. Ma and A. K. Y. Jen, *Adv. Mater.*, 2008, **20**, 2376-2382.
19. K. Asadi, F. Gholamrezaie, E. C. P. Smits, P. W. M. Blom and B. d. Boer, *J. Mater. Chem.*, 2007, **17**, 1947-1953.
20. X. Cheng, Y.-Y. Noh, J. Wang, M. Tello, J. Frisch, R.-P. Blum, A. Vollmer, J. P. Rabe, N. Koch and H. Sirringhaus, *Adv. Funct. Mater.*, 2009, **19**, 2407-2415.
21. B. H. Hamadani, D. A. Corley, J. W. Ciszek, J. M. Tour and D. Natelson, *Nano Lett.*, 2006, **6**, 1303-1306.
22. J. Lee, B.-J. Jung, J.-I. Lee, H. Y. Chu, L.-M. Do and H.-K. Shim, *J. Mater. Chem.*, 2002, **12**, 3494-3498.
23. U. Manna, H. M. Kim, M. Gowtham, J. Yi, S. Sohn and D. Jung, *Thin Solid Films*, 2006, **495**, 380-384.
24. E. Orgiu, N. Crivillers, J. Rotzler, M. Mayor and P. Samori, *J. Mater. Chem.*, 2010, **20**, 10798-10800.
25. E. L. Ratcliff, A. Garcia, S. A. Paniagua, S. R. Cowan, A. J. Giordano, D. S. Ginley, S. R. Marder, J. J. Berry and D. C. Olson, *Advanced Energy Materials*, 2013, **3**, 647-656.
26. K. M. Knesting, H. Ju, C. W. Schlenker, A. J. Giordano, A. Garcia, O. N. L. Smith, D. C. Olson, S. R. Marder and D. S. Ginger, *The Journal of Physical Chemistry Letters*, 2013, **4**, 4038-4044.
27. J. Chen, R. E. Ruther, Y. Tan, L. M. Bishop and R. J. Hamers, *Langmuir*, 2012, **28**, 10437-10445.
28. Y. E. Ha, M. Y. Jo, J. Park, Y.-C. Kang, S. I. Yoo and J. H. Kim, *J. Phys. Chem. C.*, 2013, **117**, 2646-2652.
29. Y. E. Ha, M. Y. Jo, J. Park, Y.-C. Kang, S.-J. Moon and J. H. Kim, *Synth. Met.*, 2014, **187**, 113-117.
30. P. C. Rusu, G. Giovannetti and G. Brocks, *J. Phys. Chem. C.*, 2007, **111**, 14448-14456.
31. P. C. Rusu and G. Brocks, *J. Phys. Chem. B*, 2006, **110**, 22628-22634.
32. P. C. Rusu and G. Brocks, *Phys. Rev. B*, 2006, **74**, 073414.
33. G. Heimel, L. Romaner, J.-L. Brédas and E. Zojer, *Surf. Sci.*, 2006, **600**, 4548-4562.
34. G. Heimel, L. Romaner, E. Zojer and J.-L. Bredas, *Acc. Chem. Res.*, 2008, **41**, 721-729.
35. G. Heimel, L. Romaner, E. Zojer and J.-L. Brédas, *Nano Lett.*, 2007, **7**, 932-940.
36. H. Li, Y. Duan, P. Paramonov, V. Coropceanu and J.-L. Brédas, *J. Electron Spectrosc.*, 2009, **174**, 70-77.
37. M. Gliboff, L. Sang, K. M. Knesting, M. C. Schalnat, A. Mudalige, E. L. Ratcliff, H. Li, A. K. Sigdel, A. J. Giordano, J. J. Berry, D. Nordlund, G. T. Seidler, J.-L. Brédas, S. R. Marder, J. E. Pemberton and D. S. Ginger, *Langmuir*, 2013, **29**, 2166-2174.
38. C. Wood, H. Li, P. Winget and J.-L. Brédas, *J. Phys. Chem. C.*, 2012, **116**, 19125-19133.
39. H. Li, E. L. Ratcliff, A. K. Sigdel, A. J. Giordano, S. R. Marder, J. J. Berry and J.-L. Brédas, *Adv. Funct. Mater.*, 2014, n/a-n/a.
40. O. T. Hofmann, J.-C. Deinert, Y. Xu, P. Rinke, J. Stähler, M. Wolf and M. Scheffler, *J. Chem. Phys.*, 2013, **139**, 174701.
41. S. Hovel, C. Kolczewski, M. Wuhn, J. Albers, K. Weiss, V. Staemmler and C. Woll, *J. Chem. Phys.*, 2000, **112**, 3909-3916.
42. S. Yu, S. Ahmadi, C. Sun, P. l. Palmgren, F. Hennies, M. Zuleta and M. Göthelid, *J. Phys. Chem. C.*, 2010, **114**, 2315-2320.
43. J.-Y. Kim, J. Y. Kim, D.-K. Lee, B. Kim, H. Kim and M. J. Ko, *J. Phys. Chem. C.*, 2012, **116**, 22759-22766.
44. C. Woll, *Prog. Surf. Sci.*, 2007, **82**, 55.
45. O. Dulub, L. A. Boatner and U. Diebold, *Surf. Sci.*, 2002, **519**, 201.
46. R. Triboulet and J. Perriere, *Progr. Cryst. Growth Charact. Mater.*, 2003, **47**, 65.
47. C. Y. Zhang, X. M. Li, X. Zhang, W. D. Yu and J. L. Zhao, *J. Cryst. Growth*, 2006, **290**, 67.
48. A. Wander, F. Schedin, P. Steadman, A. Norris, R. McGrath, T. S. Turner, G. Thornton and N. M. Harrison, *Phys. Rev. Lett.*, 2001, **86**, 3811.
49. G. Kresse, O. Dulub and U. Diebold, *Phys. Rev. B*, 2003, **68**, 245409.
50. B. Meyer, *Phys. Rev. B*, 2004, **69**, 045416.
51. H. Li, L. K. Schirra, J. Shim, H. Cheun, B. Kippelen, O. L. A. Monti and J.-L. Bredas, *Chem. Mater.*, 2012, **24**, 3044-3055.

52. E. Artacho, E. Anglada, O. Diéguez, J. D. Gale, A. García, J. Junquera, R. M. Martin, P. Ordejón, J. M. Pruneda, D. Sánchez-Portal and J. M. Soler, *J. Phys.: Condens. Matter*, 2008, **20**, 064208.
53. J. M. Soler, E. Artacho, J. D. Gale, A. García, J. Junquera, P. Ordejón and D. Sánchez-Portal, *J. Phys.: Condens. Matter*, 2002, **14**, 2745.
54. J. P. Perdew, K. Burke and M. Ernzerhof, *Phys. Rev. Lett.*, 1996, **77**, 3865.
55. B. G. Hyde and S. Anderson, *Inorganic Crystal Structures*, Wiley, New-York, 1989.
56. E. H. Kisi and M. M. Elcombe, *Acta Crystallogr., Sect. C*, 1989, **45**, 1867.
57. A. Baldereschi, S. Baroni and R. Resta, *Phys. Rev. Lett.*, 1988, **61**, 734-737.
58. K. Jacobi, G. Zwicker and A. Gutmann, *Surf. Sci.*, 1984, **141**, 109-125.
59. O. Yaffe, S. Pujari, O. Sinai, A. Vilan, H. Zuilhof, A. Kahn, L. Kronik, H. Cohen and D. Cahen, *J. Phys. Chem. C.*, 2013, **117**, 22422-22427.
60. P. Winget, L. K. Schirra, D. Cornil, H. Li, V. Coropceanu, P. F. Ndione, A. K. Sigdel, D. S. Ginley, J. J. Berry, J. Shim, H. Kim, B. Kippelen, J.-L. Brédas and O. L. A. Monti, *Adv. Mater.*, 2014, **26**, 4711-4716.
61. S. Nénon, R. Méreau, S. Salman, F. Castet, T. Van Regemorter, S. Clima, D. Beljonne and J. Cornil, *The Journal of Physical Chemistry Letters*, 2011, **3**, 58-63.
62. H. Ishii, K. Sugiyama, E. Ito and K. Seki, *Adv. Mater.*, 1999, **11**, 605-625.
63. I. H. Campbell, J. D. Kress, R. L. Martin, D. L. Smith, N. N. Barashkov and J. P. Ferraris, *Appl. Phys. Lett.*, 1997, **71**, 3528-3530.
64. I. H. Campbell, S. Rubin, T. A. Zawodzinski, J. D. Kress, R. L. Martin, D. L. Smith, N. N. Barashkov and J. P. Ferraris, *Phys. Rev. B*, 1996, **54**, R14321-R14324.
65. B. de Boer, A. Hadipour, M. M. Mandoc, T. van Woudenbergh and P. W. M. Blom, *Adv. Mater.*, 2005, **17**, 621-625.
66. R. W. Zehner, B. F. Parsons, R. P. Hsung and L. R. Sita, *Langmuir*, 1999, **15**, 1121-1127.
67. G. Heimel, L. Romaner, J.-L. Brédas and E. Zojer, *Phys. Rev. Lett.*, 2006, **96**, 196806 (196819).
68. S. Gutmann, M. Conrad, M. A. Wolak, M. M. Beerbom and R. Schlaf, *J. Appl. Phys.*, 2012, **111**, 123710-123717.
69. H. Xu, W. Fan, D. Fang, A. L. Rosa, T. Frauenheim and R. Q. Zhang, *physica status solidi (b)*, 2010, **247**, 2581-2593.
70. A. Beltrán, J. Andrés, M. Calatayud and J. B. L. Martins, *Chem. Phys. Lett.*, 2001, **338**, 224-230.
71. N. L. Marana, V. M. Longo, E. Longo, J. B. L. Martins and J. R. Sambrano, *J. Phys. Chem. A*, 2008, **112**, 8958-8963.
72. B. Meyer and D. Marx, *Phys. Rev. B*, 2003, **67**, 035403.
73. A. Wander and N. M. Harrison, *Surf. Sci.*, 2000, **457**, 342-346.
74. N. Jedrecy, S. Gallini, M. Sauvage-Simkin and R. Pinchaux, *Surf. Sci.*, 2000, **460**, 136-143.
75. O. Taratula, E. Galoppini, D. Wang, D. Chu, Z. Zhang, H. Chen, G. Saraf and Y. Lu, *J. Phys. Chem. B*, 2006, **110**, 6506-6515.
76. P. Persson, S. Lunell and L. Ojamäe, *Int. J. Quantum Chem*, 2002, **89**, 172-180.
77. X. Tian, J. Xu and W. Xie, *J. Phys. Chem. C.*, 2010, **114**, 3973-3980.
78. D. Cornil and J. Cornil, *J. Electron. Spectrosc. Relat. Phenom.*, 2013, **189**, 32-38.
79. L. Mei, T. Ming, L. Rong, S. Jie, Y. Zhong and L. Liang, *J Chem Sci*, 2009, **121**, 435-440.
80. J. F. Walsh, R. Davis, C. A. Muryn, G. Thornton, V. R. Dhanak and K. C. Prince, *Phys. Rev. B*, 1993, **48**, 14749-14752.
81. D. Cornil, Y. Olivier, V. Geskin and J. Cornil, *Adv. Funct. Mater.*, 2007, **17**, 1143-1148.
82. M. L. Sushko and A. L. Shluger, *Adv. Funct. Mater.*, 2008, **18**, 2228-2236.
83. D. Cahen, R. Naaman and Z. Vager, *Adv. Funct. Mater.*, 2005, **15**, 1571-1578.
84. L. Romaner, G. Heimel, C. Ambrosch-Draxl and E. Zojer, *Adv. Funct. Mater.*, 2008, **18**, 3999-4006.
85. N. Crivillers, S. Osella, C. Van Dyck, G. M. Lazzerini, D. Cornil, A. Liscio, F. Di Stasio, S. Mian, O. Fenwick, F. Reinders, M. Neuburger, E. Treossi, M. Mayor, V. Palermo, F. Cacialli, J. Cornil and P. Samorì, *Adv. Mater.*, 2013, **25**, 432-436.
86. Y. Wang, M. Muhler and C. Woll, *PCCP*, 2006, **8**, 1521-1524.
87. H. Noei, H. Qiu, Y. Wang, E. Loffler, C. Woll and M. Muhler, *PCCP*, 2008, **10**, 7092-7097.
88. K. Ozawa and K. Mase, *Phys. Rev. B*, 2010, **81**, 205322 (205324).
89. Y. Wang, B. Meyer, X. Yin, M. Kunat, D. Langenberg, F. Traeger, A. Birkner and C. Wöll, *Phys. Rev. Lett.*, 2005, **95**, 266104 (266104).
90. , Prof. Mats Fahlman, private communication.